Stability of the MUSCL Method on General Unstructured Grids for Applications to Compressible Fluid Flow

F. Haider[1], Jean-Pierre Croisille[2], and B. Courbet[1]

[1] ONERA Département de simulation numérique des écoulements et aéroacoustique
29 rue de la Division Leclerc 92320 Châtillon FRANCE
florian.haider@onera.fr, bernard.courbet@onera.fr

[2] Laboratoire Mathématiques et Applications, UMR 7122, Université Paul Verlaine Bât. A, Ile du Saulcy 57045 Metz FRANCE
jean-pierre.croisille@math.univ-metz.fr

1 Introduction

In recent years, practical applications have motivated various extensions of the MUSCL finite-volume method to general unstructured meshes and the MUSCL approach is at the heart of many solvers for compressible gas dynamics. On unstructured grids, many stability results rely explicitly on slope limiters, see for example the maximum principle in [BO04] and the convergence results in [Cha00, Kro97]. Limiters are inherently non-linear methods in the sense that they give non-linear schemes even when they are applied to linear equations. Their importance lies mainly in applications to non-linear gas dynamics involving steep gradients and shocks. However, in order to analyze the properties of a numerical scheme, it remains important to study its behaviour in the case of the linear advection equation. In the absence of slope limiters, the spatial discretization of the linear advection equation with constant coefficients results in a linear semi-discrete equation.

The purpose of the present work is a theoretical and numerical analysis of this semi-discrete equation in order to examine the influence of the grid type, the reconstruction method and the stencil size on the linear stability of the MUSCL scheme on unstructured grids. The goal is to identify the slope reconstruction methods and the stencil sizes that lead to stable discretizations of linear advection. In applications to compressible gas dynamics, MUSCL schemes using these methods can be expected to be more robust and accurate than schemes that are stabilized only by slope limiters. Furthermore, it is interesting to examine if such schemes can be used with limiters that are less restrictive than the limiters presented for example in [BO04]. The present study is motivated by extensive numerical experiments in three-dimensional applications to internal flows and aerothermochemistry with the package CEDRE developed by ONERA. We refer to [HCC08, Hai08] for more details.

2 Slope Reconstruction on General Unstructured Meshes

This section develops the geometric notation and a general approach to consistent slope reconstruction on unstructured grids. Throughout this paper the boundary conditions are assumed to be periodic. We consider a general unstructured grid of a cube $\Omega \subseteq \mathbb{R}^d$ consisting of N general polyhedra $\mathcal{T}_\alpha$ with barycenter $\mathbf{x}_\alpha$ and d-volume $|\mathcal{T}_\alpha|$. The face $\mathcal{A}_{\alpha\beta}$, with barycenter $\mathbf{x}_{\alpha\beta}$, has a normal vector $\mathbf{n}_{\alpha\beta}$ oriented from cell $\mathcal{T}_\alpha$ to $\mathcal{T}_\beta$. The length of $\mathbf{n}_{\alpha\beta}$ equals the surface $|\mathcal{A}_{\alpha\beta}|$. The set of the cell indices of the direct neighbors of cell $\mathcal{T}_\alpha$ is denoted $\mathbb{V}_\alpha$. Furthermore, we define $\mathbf{h}_{\alpha\beta} = \mathbf{x}_\beta - \mathbf{x}_\alpha$ for all cells $\mathcal{T}_\alpha$ and $\mathcal{T}_\beta$ and $\mathbf{k}_{\alpha\beta} = \mathbf{x}_{\alpha\beta} - \mathbf{x}_\alpha$ for all adjacent cells $\mathcal{T}_\alpha$ and $\mathcal{T}_\beta$. Whenever two cells have no common interface, $\mathbf{n}_{\alpha\beta} \triangleq 0$ and $\mathbf{k}_{\alpha\beta} \triangleq 0$. In addition, $\mathbf{n}_{\alpha\alpha} \triangleq 0$, $\mathbf{k}_{\alpha\alpha} \triangleq 0$ and $\mathbf{h}_{\alpha\alpha} \triangleq 0$. This allows to drop the neighborhood in all sums and to write $\sum_\beta$ instead of $\sum_{\beta \in \mathbb{V}_\alpha}$. The reconstruction of a slope $\boldsymbol{\sigma}_\alpha$ in each cell $\mathcal{T}_\alpha$ allows to compute second order accurate values

$$u_{\alpha\beta} = u_\alpha + \boldsymbol{\sigma}_\alpha \cdot \mathbf{k}_{\alpha\beta} \tag{1}$$

at the barycenter $\mathbf{x}_{\alpha\beta}$ of the cell interface $\mathcal{A}_{\alpha\beta}$. The most general linear slope reconstruction method can be written as

$$\mathfrak{u} \mapsto \boldsymbol{\sigma}_\alpha(\mathfrak{u}) = \sum_\beta \mathbf{s}_{\alpha\beta}(u_\beta - u_\alpha) \tag{2}$$

where the $\mathbf{s}_{\alpha\beta}$ are coefficient vectors in cell $\mathcal{T}_\alpha$ and $\mathbf{s}_{\alpha\beta} \triangleq 0$ by definition if cell $\mathcal{T}_\beta$ is not in the reconstruction stencil of cell $\mathcal{T}_\alpha$. Second order accuracy requires that (2) reproduce the slope of polynomials of degree one. This is equivalent to the following consistency condition for the coefficients $\mathbf{s}_{\alpha\beta}$

$$\boldsymbol{\sigma} = \sum_\beta \mathbf{s}_{\alpha\beta}\ (\mathbf{h}_{\alpha\beta} \cdot \boldsymbol{\sigma}) \quad \text{ for all } \boldsymbol{\sigma} \in \mathbb{R}^d\,. \tag{3}$$

Let m be the number of cells in the reconstruction stencil of cell $\mathcal{T}_\alpha$ and $\mathbb{W}_\alpha \triangleq \{\beta_1, \beta_2, \ldots, \beta_m\}$ the cell indices in that stencil. On cell $\mathcal{T}_\alpha$, the unknown vectors $\mathbf{s}_{\alpha\beta}$, $\beta \in \mathbb{W}_\alpha$, form the columns of a $d \times m$ matrix S_α. Similarly, the vectors $\mathbf{h}_{\alpha\beta}$, $\beta \in \mathbb{W}_\alpha$, form the rows of the $m \times d$ matrix H_α. Now the consistency condition (3) can be written as the matrix equation with unknown S_α

$$S_\alpha H_\alpha = \mathrm{I}_{d\times d}\,. \tag{4}$$

The least-squares slope coincides with the pseudo-inverse of H_α that is also the minimum Frobenius norm solution of (4), see [HCC08]. It is given by

$$S_\alpha^{\mathrm{ls}} = \left(H_\alpha^t H_\alpha\right)^{-1} H_\alpha^t\,.$$

Another method is based on the well-known Green Theorem and results in

$$S_\alpha^{\mathrm{gr}} = \left(N_\alpha^t H_\alpha\right)^{-1} N_\alpha^t$$

where the matrix N_α has the row vectors

$$\mathbf{n}'_{\alpha\beta} = \frac{\|\mathbf{a}_{\alpha\beta}\|}{\|\mathbf{h}_{\alpha\beta}\|}\mathbf{n}_{\alpha\beta}$$

and $\mathbf{a}_{\alpha\beta}$ is the orthogonal projection of $\mathbf{k}_{\alpha\beta}$ on $\mathbf{h}_{\alpha\beta}$, see [HCC08].

3 Stability Analysis of the MUSCL Scheme

The application of the semi-discrete MUSCL scheme to the linear advection equation $\partial_t u(\mathbf{x},t) + \mathbf{c}\cdot\boldsymbol{\nabla} u(\mathbf{x},t) = 0$ with periodic boundary condition results in a linear dynamical system (*method of lines*)

$$\frac{\mathrm{d}u_\alpha(t)}{\mathrm{d}t} = \sum_\beta J_{\alpha\beta} u_\beta(t)\ ;\ 1 \le \alpha \le N. \tag{5}$$

The definition $\mathbf{s}_\alpha \triangleq \sum_\beta \mathbf{s}_{\alpha\beta}$ allows to write the MUSCL operator J in (5) as

$$\begin{aligned} J_{\alpha\beta} = -|\mathcal{T}_\alpha|^{-1} \Bigg\{ & \sum_\gamma (\mathbf{c}\cdot\mathbf{n}_{\alpha\gamma})_+ \delta_{\alpha\beta} + (\mathbf{c}\cdot\mathbf{n}_{\alpha\beta})_- + \\ & + \sum_\gamma (\mathbf{n}_{\alpha\gamma}\cdot\mathbf{c})_+ \mathbf{k}_{\alpha\gamma}\cdot\mathbf{s}_{\alpha\beta} - \sum_\gamma (\mathbf{n}_{\alpha\gamma}\cdot\mathbf{c})_+ \mathbf{k}_{\alpha\gamma}\cdot\mathbf{s}_\alpha\,\delta_{\alpha\beta} - \\ & - \sum_\gamma (\mathbf{n}_{\gamma\alpha}\cdot\mathbf{c})_+ \mathbf{k}_{\gamma\alpha}\cdot\mathbf{s}_{\gamma\beta} + (\mathbf{n}_{\beta\alpha}\cdot\mathbf{c})_+ \mathbf{k}_{\beta\alpha}\cdot\mathbf{s}_\beta \Bigg\}\ . \end{aligned} \tag{6}$$

The time derivative of the quadratic energy function of (5) can be written as a sum

$$\frac{\mathrm{d}}{\mathrm{d}t}E(t) = \sum_{\alpha=1}^{N} |\mathcal{T}_\alpha| \frac{\mathrm{d}}{\mathrm{d}t}\left(|u_\alpha(t)|^2\right) = \sum_{\alpha=1}^{N} \Phi_\alpha(\mathfrak{u}) \tag{7}$$

where

$$\begin{aligned} \Phi_\alpha(\mathfrak{u}) = \sum_\beta (\mathbf{c}\cdot\mathbf{n}_{\alpha\beta})_+ \Bigg[& \underbrace{-(u_\beta - u_\alpha)^2}_{\mathrm{I}} + \\ & \underbrace{+2\sum_\gamma (u_\beta - u_\alpha)\, r^{(\alpha)}_{\beta\gamma}\, (u_\gamma - u_\alpha)}_{\mathrm{II}} \Bigg]\ . \end{aligned} \tag{8}$$

Note that the first term is always non-positive whereas the second term can be positive. The elements $r^{(\alpha)}_{\beta\gamma} \triangleq \mathbf{k}_{\alpha\beta}\cdot\mathbf{s}_{\alpha\gamma}$ in the second part of (8) form the entries

of a local geometric matrix R_α attached to the cell $\mathcal{T}_\alpha$. If K_α is the matrix whose rows are the vectors $\mathbf{k}_{\alpha\beta}$ for $\beta \in \mathbb{V}_\alpha$ then $R_\alpha = K_\alpha S_\alpha$. The dimensionless operator R_α is invariant under scaling of the grid and defines the linear mapping $R_\alpha : (u_\gamma - u_\alpha)_{\gamma\in\mathbb{W}_\alpha} \mapsto (u_{\alpha\beta} - u_\alpha)_{\beta\in\mathbb{V}_\alpha}$ where $u_{\alpha\beta}$ is defined by (1). We summarize the main results of our study, see [HCC08, Hai08], as follows.

Theorem 1 (Stability of the First Order Finite Volume Scheme). *If all reconstruction coefficients $\mathbf{s}_{\alpha\gamma}$ are zero then $\frac{d}{dt}E(t) \leq 0$ on arbitrary polyhedral meshes regardless of the velocity $\mathbf{c}$ and the space dimension d.* □

Theorem 1 and (8) suggest to choose reconstruction coefficients that minimize an appropriate matrix norm of $R_\alpha = K_\alpha S_\alpha$ under the constraint (4).

Theorem 2 (Minimization Property of the Least-squares Reconstruction). *The least-squares reconstruction minimizes each singular value of $K_\alpha S_\alpha$ and therefore all unitarily invariant matrix norms, in particular the Spectral, Frobenius, and the Trace norms among the matrices satisfying (4).*

For the least squares reconstruction, the influence of the stencil size on the matrix R_α is characterized by

Theorem 3 (Influence of the Stencil Size on the Reconstruction Matrix). *Let $\tilde{S}_\alpha$ be the least-squares slope reconstruction matrix. If cells are added to the reconstruction stencil, then the singular values as well as all unitarily invariant matrix norms of $R_\alpha = K_\alpha\tilde{S}_\alpha$ are non-increasing. Furthermore, if $\{\beta_1, \ldots, \beta_k\}$ are the indices of the newly added cells and if the family of vectors $\{\mathbf{h}_{\alpha\beta_1}, \ldots, \mathbf{h}_{\alpha\beta_k}\}$ has full rank d then all unitarily invariant matrix norms as well as all strictly positive singular values of $R_\alpha = K_\alpha\tilde{S}_\alpha$ are strictly decreasing.*

Theorems 2 and 3 allow the following practical conclusions that have been tested numerically in Sect. 4. First, the least-squares reconstruction should provide better stability than alternative reconstruction methods. Second, larger stencil sizes should increase the linear stability of the MUSCL scheme.

4 Numerical Computation of Spectra of MUSCL Operators

This section presents the numerical computations of spectra of (6) for two- and three-dimensional grids on the unit square and the unit cube. The purpose of these calculations is to look for a correlation between the values of R_α and the appearance of unstable eigenmodes and to test the conclusions at the end of Sect. 3. The test cases include different grid types, reconstruction methods and stencil sizes. A program written in MAPLE computes for each test case the matrix of (6) and its spectral abscissa, defined by $\omega_J = \max\{\Re(\lambda) | \lambda \in \sigma(J)\}$ as well as the spectral norm of $R_\alpha = K_\alpha S_\alpha$ for each cell $\mathcal{T}_\alpha$. The numerical computations reveal a strong correlation between the values of R_α and the existence of unstable eigenvalues λ with $\Re(\lambda) > 0$. The latter appear only on grids with cells where the spectral norm of

R_α approaches or exceeds 1. Recall that the matrix R_α is dimensionless and scaling invariant. The case where the largest values of R_α have been observed is the first neighborhood slope reconstruction in three dimensions on tetrahedra and prisms. For this case, the least-squares as well as the Green slope produce a small number of unstable eigenmodes. For second neighborhood stencils, the second order accurate slope can also produce unstable modes on tetrahedra that appear together with values of $\|R_\alpha\| > 1$. For all other cases, the values of $\|R_\alpha\|$ are smaller than 1 and no unstable modes occur.

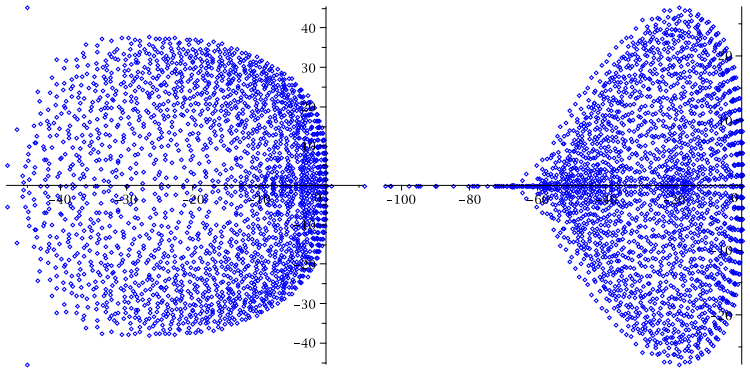

(a) First neighborhood (b) Second neighborhood

Fig. 1. Spectra of the operator (6) for a tetrahedral grid : Least-squares reconstruction on the first and second neighborhood. For the former, two unstable eigenmodes are visible on the right of the imaginary axis

5 Applications to Compressible Gas Dynamics

The conclusions of Sect. 3 have been put in practice to enhance the flow solver CEDRE. However, for an industrial software like CEDRE that is built to handle large unstructured grids by parallelization it is preferable to avoid the implementation issues of large reconstruction stencils. We have therefore adopted a different method that can be coded by means of the first neighborhood connectivity only. In a first step, the algorithm computes in each cell a slope using the least-squares reconstruction on the first neighborhood. In a second step, the algorithm takes a weighted average of these slopes over the first neighbors of each cell. Numerical computations of spectra for the convection operator (6) show that this leads to a stable MUSCL discretization of the linear advection equation. This slope reconstruction method has recently been tested with CEDRE on unstructured grids for the subsonic flow over a deep 3D

cavity and for a supersonic jet, see [LSM03, LRV05]. In the case of the flow over a cavity, the scheme is stable with the new slope reconstruction without any limitation on tetrahedral grids. Previously, this was only the case for simulations on structured meshes. In the case of the jet, a slope limiter is still needed due to the presence of steep temperature and pressure gradients but the simulation could be carried out with a limiter that is less restrictive than the maximum principle presented in [BO04]. This is impossible without the linear stability of the new robust reconstruction.

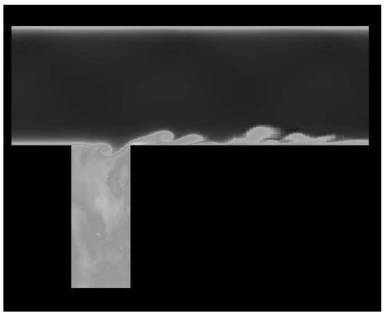

Fig. 2. Entropy for the flow over a deep 3D cavity, see [LSM03]

References

[BO04] Barth, T., Ohlberger, M.: Finite Volume Methods: Foundation and Analysis. In: Stein, E., De Borst, R. , Hughes, T.J.R. (ed) Encyclopedia of Computational Mechanics. Wiley, New York (2004)

[Cha00] Chainais-Hillairet, C.: Second Order Finite Volume Schemes for a Nonlinear Hyperbolic Equation : Error Estimate. Math. Meth. Appl. Sci., **23** (5) : 467–490 (2000)

[HCC08] Haider, F., Croisille, J.P., Courbet, B.: Stability Analysis of the Cell Centered Finite-Volume MUSCL Method on Unstructured Grids. Submitted (2008)

[Hai08] Haider, F.: Discrétisation en maillage non structuré et applications LES. Thesis, University Paris 6 (2008)

[Kro97] Kröner, D.: Numerical Schemes for Conservation Laws. John Wiley and Sons, Chichester, and B.G. Teubner, Stuttgart (1997)

[LSM03] Larchevêque, L., Sagaut, P., Mary, I., Labbé, O., Comte, P.: Large-eddy simulation of the compressible flow over a deep, open cavity. Phys. Fluids 15(1), 193-210 (2003)

[LRV05] Lupoglazoff N., Rahier G., Vuillot F. Application of the CEDRE Unstructured Flow Solver to Jet Noise Computations. First European Conference for Aerospace Sciences (EUCASS), Moscou, Russie (2005)